

Observation of First-Order Quantum Phase Transitions and Ferromagnetism in Twisted Double Bilayer Graphene

Le Liu,^{1,2,‡} Xin Lu,^{3,‡} Yanbang Chu,^{1,2} Guang Yang,^{1,2} Yalong Yuan,^{1,2} Fanfan Wu,^{1,2} Yiru Ji,^{1,2} Jinpeng Tian,^{1,2} Kenji Watanabe[Ⓞ],⁴ Takashi Taniguchi,⁵ Luojun Du,^{1,2} Dongxia Shi,^{1,2,6} Jianpeng Liu,^{3,7} Jie Shen,^{1,2,6} Li Lu,^{1,2,6} Wei Yang[Ⓞ],^{1,2,6,*} and Guangyu Zhang[Ⓞ]^{1,2,6,†}

¹Beijing National Laboratory for Condensed Matter Physics and Institute of Physics, Chinese Academy of Sciences, Beijing 100190, China

²School of Physical Sciences, University of Chinese Academy of Sciences, Beijing, 100190, China

³School of Physical Sciences and Technology, ShanghaiTech University, Shanghai 200031, China

⁴Research Center for Functional Materials, National Institute for Materials Science, 1-1 Namiki, Tsukuba 305-0044, Japan

⁵International Center for Materials Nanoarchitectonics, National Institute for Materials Science, 1-1 Namiki, Tsukuba 305-0044, Japan

⁶Songshan Lake Materials Laboratory, Dongguan 523808, China

⁷ShanghaiTech Laboratory for Topological Physics, ShanghaiTech University, Shanghai 200031, China

 (Received 13 March 2023; revised 5 June 2023; accepted 22 June 2023; published 7 August 2023)

Twisted graphene multilayers are highly tunable flatband systems for developing new phases of matter. Thus far, while orbital ferromagnetism has been observed in valley-polarized phases, the long-range orders of other correlated phases as well as the quantum phase transitions between different orders mostly remain unknown. Here, we report an observation of Coulomb-interaction-driven first-order quantum phase transitions and ferromagnetism in twisted double bilayer graphene (TDBG). At zero magnetic field, the transitions are revealed in a series of steplike abrupt resistance jumps with a prominent hysteresis loop when either the displacement field (D) or the carrier density (n) is tuned across a symmetry-breaking boundary near half filling, indicating a formation of ordered domains. It is worth noting that the good tunability and switching of these states give rise to a memory performance with a large on/off ratio. Moreover, when both spin and valley play the roles at finite magnetic field, we observe abundant first-order quantum phase transitions among normal metallic states from the charge-neutral point, orbital ferromagnetic states from quarter filling, and spin-polarized states from half filling. We interpret these first-order phase transitions in the picture of phase separations and spin-domain percolations driven by multifield tunable Coulomb interactions, in agreement with the Lifshitz transition and the Hartree-Fock calculations. The observed multifield tunable domain structure and its hysteresis resembles the characteristics of multiferroics, revealing intriguing magnetoelectric properties. Our result enriches the correlated phase diagram in TDBG for discovering novel exotic phases and quantum phase transitions, and it will benefit other twisted moiré systems as well.

DOI: [10.1103/PhysRevX.13.031015](https://doi.org/10.1103/PhysRevX.13.031015)

Subject Areas: Magnetism, Mesoscopics,
Strongly Correlated Materials

I. INTRODUCTION

Phase transitions are expected to occur at the instability when thermodynamic properties (density of states, susceptibility, or compressibility) or quasiparticle scattering rates diverge. In the strong-coupling regime, i.e., $U/W \geq \sim 1$ where U is the Coulomb repulsion energy and W is the kinetic energy, a rich interplay of charge, spin, and orbital degrees of freedom contribute to versatile symmetry-breaking phase diagrams where different correlated orders compete or coexist. Twisted graphene multilayers emerge as highly tunable flatband systems to realize these exotic phases, such as correlated insulators [1–9], superconductivity [10–17], and magnetism [7,8,11,18–22]. In these

*Corresponding author.
wei.yang@iphy.ac.cn

†Corresponding author.
gyzhang@iphy.ac.cn

‡These authors contributed equally to this work.

Published by the American Physical Society under the terms of the [Creative Commons Attribution 4.0 International license](https://creativecommons.org/licenses/by/4.0/). Further distribution of this work must maintain attribution to the author(s) and the published article's title, journal citation, and DOI.

flatband systems, the presence of van Hove singularities (VHSs) [3,9,12,23] and cascade transitions [24–26] contribute significantly to instabilities that lead to the symmetry-breaking isospin polarizations and the resulted delicate ground states. Thus far, orbital ferromagnetism with magnetic domains have been observed in valley-polarized phases [7,8,11,18–22] where Coulomb interaction and band topology play important roles. However, the long-range order of other correlated phases mostly remains unknown. In particular, the spin-related phenomena are rare, and direct evidence of the magnetic order of the spin-polarized insulator has not been observed yet.

Here, we focus on the instability of a phase diagram when spin fluctuations are critical in the vicinity of a spin-polarized correlated insulator in twisted double bilayer graphene (TDBG). With unique spin-polarized correlated insulators [2–5] and VHS-like phase boundary [3,23], TDBG is an excellent platform to study the spin-related phases and phase transitions. Importantly, by sweeping the carrier density n or displacement field D back and forth,

we observe first-order phase transitions at zero magnetic field with a series of Barkhausen-like resistance jumps and electrical hysteresis. We further demonstrate the dominant role of the spin order by performing both in-plane and out-of-plane magnetotransport measurements, and interpret these first-order phase transitions in the picture of correlation-driven spin-domain percolations. In addition, we observe abundant first-order phase transitions among normal metallic states from the charge-neutral point, orbital ferromagnetic states from quarter filling, and spin-polarized states from half filling.

II. RESULTS

A. D -field and doping-tunable first-order phase transitions with hysteresis at $B = 0$ T

Figure 1(a) shows a typical phase diagram at $T = 30$ mK, i.e., a color mapping of longitudinal resistance R_{xx} as a function of n and D , for the TDBG device with a twisted angle of 1.35° , and Fig. 1(b) is the corresponding R_{xy} at a

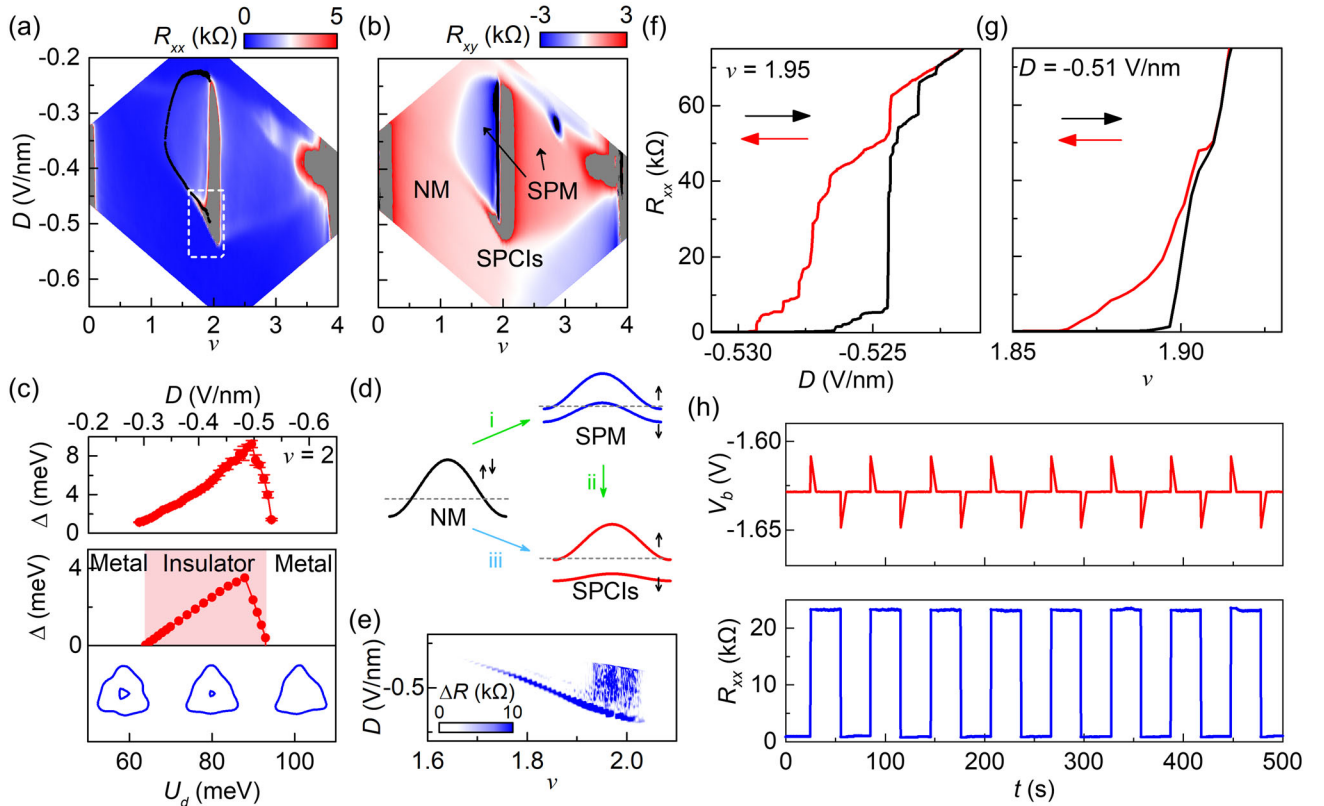


FIG. 1. Gate-voltage-driven first-order phase transitions at the halo boundary. (a),(b) R_{xx} and R_{xy} maps as a function of ν and D . The Hall resistance is measured at $B_{\perp} = 1$ T. The black dots in (a) correspond to the points of $R_{xy} = 0$ in (b). (c) Top panel: thermal activation energy gaps versus D at $\nu = 2$. Bottom panel: calculated correlated gap as a function of interlayer potential difference U_d at $\nu = 2$. The corresponding noninteracting Fermi surfaces are depicted in blue lines. (d) Schematics of different phases in (a) and (b). i, ii, iii correspond to phase transitions among the three phases of NM, SPCIs, and SPM. Black arrows correspond to directions of spin. Gray dashed lines correspond to Fermi levels. (e) ΔR maps limited in the white dashed box of (a). (f),(g) D - and doping-driven hysteresis loops. The black (red) line corresponds to the forward (backward) sweep direction. (h) Transitions between low- and high-resistance states by applying a sequential pulse voltage on the back gate.

small magnetic field. The mappings reveal a correlated insulator at half filling in the moiré conduction band ($\nu = 2$) surrounded by a halolike structure, consistent with previous works [2–5,23,27]. Such correlated states have been regarded as the signature of spontaneous symmetry breaking [3,23] in which spin degeneracy is lifted inside the halo. The halo structure being a phase boundary separates two kinds of phases: the normal metal (NM) outside the halo and the correlated states inside the halo. Accompanied by symmetry breaking, the band structure will be reconstructed by electron-electron interaction [28] leading to the spin-polarized metal (SPM, at $\nu \neq 2$) or the spin-polarized correlated insulators (SPCIs, at $\nu = 2$) as shown schematically in Fig. 1(d). When the Fermi level is tuned across the halo boundary at $\nu < 2$, the Fermi pocket changes from electron-type to hole-type with vanishing R_{xy} at the boundary, depicted by the white contour in Fig. 1(b) and corresponding black contour in Fig. 1(a). These transport behaviors are related to the saddle-point-type VHS, at which the density of states (DOS) diverges. The topology of Fermi surface changes when the Fermi level crosses VHS, known as the Lifshitz transition. As shown in Fig. 1(c), the transport gap at $\nu = 2$ grows with $|D|$ from 0.2 to 0.5 V/nm slowly and then drops rapidly to zero within a range of 0.05 V/nm. The different trends on two sides suggest an abrupt phase transition between SPCIs and normal metal at large $|D|$. These observations are coincident with our Hartree-Fock calculations which show a sharp decreasing correlated gap. These results strongly suggest a first-order phase transition occurring between normal metal and SPCIs [iii in Fig. 1(d)] at large $|D|$.

Smoking-gun evidence of the first-order phase transition at $B = 0$ T is revealed in the transfer curves when the gate voltages are swept back and forth in the white dashed box of Fig. 1(a). In Figs. 1(f) and 1(g), the longitudinal resistance R_{xx} shows a hysteresis loop as D or ν sweeps across the phase boundary in opposite directions. This loop is independent of the sweep speed of the gate voltage (Supplemental Material Note 2 [29]), and yet is sensitive to activating current (Supplemental Material Note 3 [29]) and temperature (Supplemental Material Note 6 [29]), demonstrating an intrinsic first-order phase transition between normal metal and SPCIs. In addition, multiple jumps, most likely Barkhausen jumps [30], in hysteresis loops indicate the formation of orderly domains. Note that the abrupt transitions as well as the hysteresis at zero magnetic fields are well reproduced in a separate TDBG device D2 with a twist angle of 1.21° (Supplemental Material Note 9 [29]). Considering the spin polarization of the insulator, we conclude that there exist multiple spin-polarized ferromagnetic insulating domains in this regime. By taking the difference $\Delta R = |R_{xx}(+) - R_{xx}(-)|$ where $+/-$ represents the sweep direction, we map out the regime where first-order phase transitions occur, shown by the blue color in Fig. 1(e), along the halo boundary from $\nu = \sim 2$ to

$\nu = \sim 1.7$. Notably, the transition regime is intimately related to the VHS in single-particle band structure calculated by a continuum model [bottom panel of Fig. 1(c)]. The Fermi surface at $\nu = 2$ changes from annular with two pockets for medium interlayer potential difference U_d (60–80 meV) to a simple surface with one single electron-type pocket for large $U_d > 80$ meV. This coincidence suggests the divergent DOS across the Lifshitz transition plays a crucial role in the first-order phase transition, with the satisfied Stoner criteria $U * \text{DOS}(E_F) > 1$ (U stands for the correlation strength) inducing ferromagnetic instabilities of Fermi surfaces [31–34].

As an initial demonstration, we show that such stable and gate-tunable first-order transitions could be useful for memory. This is achieved by applying a pulse voltage on the back gate in the phase-transition regime. As shown in Fig. 1(h), a pulse voltage as small as 20 mV could induce a transition between the low-resistance state of a few hundred ohms (Ω) and high-resistance state of approximately 22 k Ω with highly tunable nature. The switching of such resistance states suggests that TDBG is a potential candidate for the memory devices working at cryogenic temperature.

B. Ferromagnetic first-order phase transitions

In addition to the D -driven and the doping-driven ones, we also observe magnetic field B -driven hysteresis. Let us first focus on the perpendicular magnetic field (B_\perp) dependence for a fixed $\nu = 1.95$ in Fig. 2(a), where the upper panel shows a color mapping of $R_{xx}(D, B_\perp)$ at $T = 100$ mK, and the lower panel is a corresponding hysteresis $\Delta R(D, B_\perp)$. Clearly, decent nonzero ΔR exists only at a low magnetic field smaller than 1.5 T, and it follows the boundary that separates the metallic states with low resistances and the insulating states with high resistances in the phase diagram. Figure 2(d) shows one representative $R(B)$ curve at $D = -0.527$ V/nm, and it gives a pronounced resistance hysteresis loop when the sweeping direction of B_\perp is changed. The hysteresis includes multiple steplike transitions, indicating the formation of multiple ferromagnetic insulating domains, and the whole loop is mirror symmetric with respect to $B = 0$ T. For a comparison, we perform similar measurements at parallel magnetic fields (B_\parallel) for a fixed $\nu = 1.95$ in the same range of D , as shown in Figs. 2(b) and 2(e). The resulted phase diagram and the hysteresis loop at B_\parallel are identical to those at $B_\perp < 1.5$ T, suggesting that the magnetic first-order transitions and the hysteresis are due to spin degrees of freedom, instead of orbital.

The origin of spin order is further supported by the vanishing hysteresis and the reverse direction of phase boundary at $B_\perp > 1.5$ T, as well as the lower R or ΔR at B_\perp compared to those at B_\parallel , where the orbital Zeeman effect competes with the spin polarization [21,35]. The details of the isospin competition are discussed later in the observation of other first-order phase transitions.

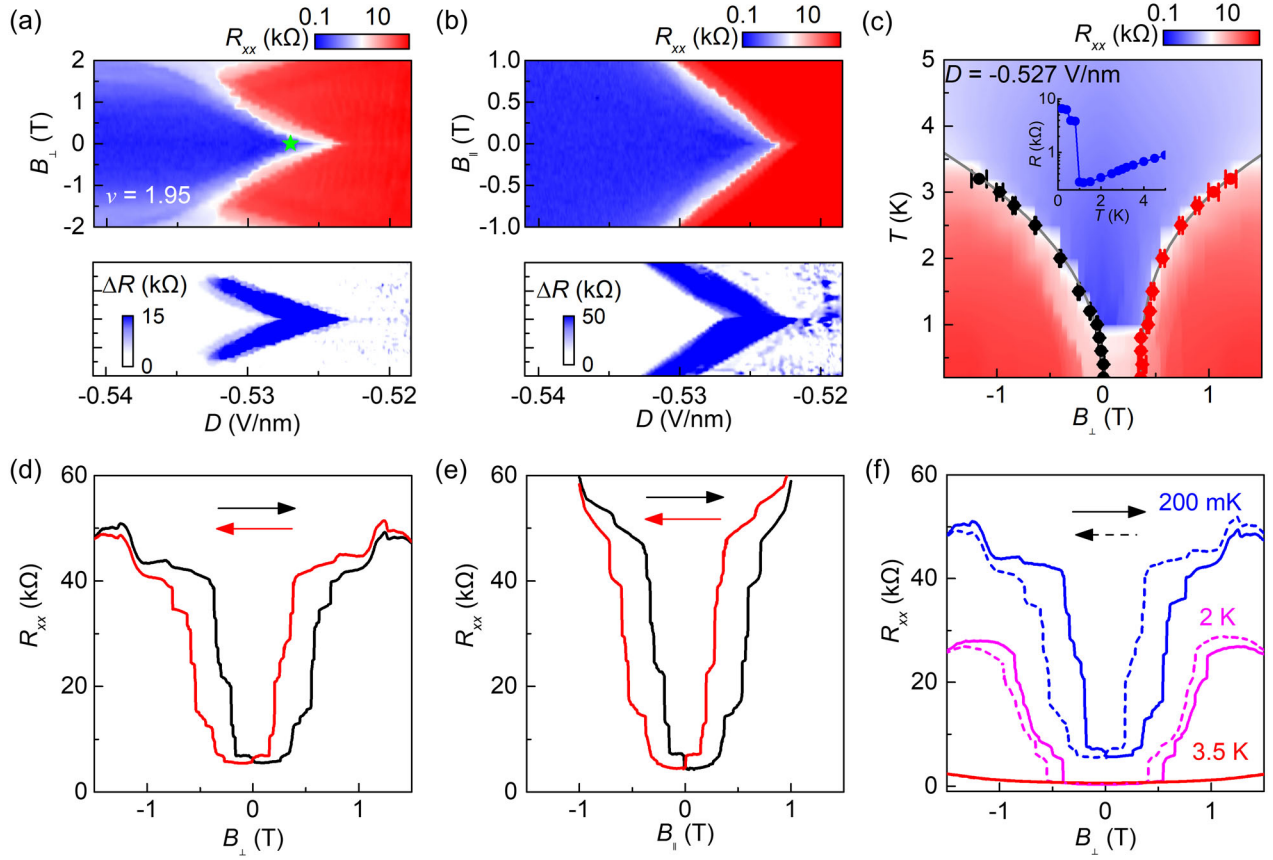


FIG. 2. Spin-polarized ferromagnetic insulators. (a) R_{xx} and ΔR as a function of D and B_{\perp} at $\nu = 1.95$. (b) R_{xx} and ΔR as a function of D and B_{\parallel} at $\nu = 1.95$. (c) R_{xx} as a function of B_{\perp} and T at $\nu = 1.95$ and $D = -0.527$ V/nm. Critical magnetic fields B_c are marked by black ($B_{\perp} < 0$) and red ($B_{\perp} > 0$) points. The gray line corresponds to the power-law fitting. Inset: R_{xx} versus T at $B_{\perp} = 0$. (d),(e) B_{\perp} - and B_{\parallel} -driven hysteresis loops at $D = -0.527$ V/nm and $T = 100$ mK marked by the green star in (a). (f) B -driven hysteresis loops at different temperatures. The solid (dashed) line corresponds to the forward (backward) sweep direction.

C. Instabilities of the first-order transitions

The first-order transitions and the hysteresis are suppressed with increasing T . For instance, the B -driven hysteresis reduces as T is increased, and it totally disappears at $T = 3.5$ K in Figs. 2(c) and 2(f); similarly, the D -driven hysteresis at $B = 0$ T disappears at around $T \sim 2.5$ K (Supplemental Material Note 6 [29]). The suppression is also observed when the applied current (I) is increased [Supplemental Material Figs. 2(a)–2(c) [30]]. Aside from the suppression of hysteresis, it needs a bigger critical field to realize the first-order transition when the T or I is increased. For instance, at $\nu = 1.95$ and $D = -0.527$ V/nm, the critical fields (B_c) of the B -driven first-order transitions are revealed in the $R(B_{\perp}, T)$ mapping in Fig. 2(c), where B is swept from negative to positive, and T is swept from low to high temperature. Note that there are two critical fields, a smaller B_{c1} (negative) for the insulator-to-metal transition and a bigger one B_{c2} (positive) for the metal-to-insulator transition indicated as the black and the red dots in Fig. 2(c), respectively. The critical field follows a power-law

relation, i.e., $B_c - B_0 \sim T^{\alpha}$, where B_0 is the critical field at the zero-temperature limit, and α represents the power-law coefficient. The critical field corresponds to the minimum spin Zeeman energy $1/2g_s\mu_B B_c$ for nucleation of ferromagnetic insulating domains, while the temperature represents the minimum thermal fluctuation $k_B T$ to break the ferromagnetic order. Here, $g_s = 2$ is the spin g factor, μ_B is the Bohr magneton, and k_B is the Boltzmann constant. We find that B_0 is around zero for B_{c1} and a nonzero value for B_{c2} , and α is between 2 and 3 for both B_{c1} and B_{c2} . It is notable that almost the same α is observed in another device D2 (Supplemental Material Note 9 [29]), suggesting a universal role in this critical phenomenon. Last but not least, the zero-field resistance $R_{xx}(B = 0$ T) in Fig. 2(c) shows an insulatinglike behavior at $T < 1$ K of approximately 6 k Ω , and then it suddenly drops below 300 Ω at $T = 1$ K, showing a metallic behavior at $T > 1$ K; alternatively, such an insulator-to-metal transition could also be achieved at $T < 1$ K by applying a large current of 50 nA, as shown in Supplemental Material Note 2 [29].

D. Phase separation and percolations of spin-ordered domains

The first-order transitions and the hysteresis driven by either displacement, carrier density, or magnetic field are observed at metal-insulator transition [36] and could be interpreted within a picture of phase separation [37,38]. The free energy of first-order transitions could have multiple local minimum points in the order parameter space, with a stable state at zero and a metastable state at finite value (Supplemental Material Note 7 [29]). The instability of the phase diagram is driven by an interplay of U/W (which can be effectively tuned by D and n) and magnetic field, which favors the domain nucleation and growth, against thermal energy as well as the couplings between domains and the surrounding metallic electron sea, which melts the domains.

The D -field-dependent first-order phase transitions are captured qualitatively in the abovementioned model. First, away from the phase boundary [Fig. 3(a)], it is a metallic state with $R < 3$ k Ω and no hysteresis. This agrees with a reduced U/W away from the halo boundary, where negligible ferromagnetic insulating domains are surrounded by metallic electron sea, and thus the electrical conduction is dominated by metallic electrons. Then, as D approaches the phase boundary [Fig. 3(b)], it becomes a metastable insulating state with $R_{xx} \sim 10$ k Ω at $B = 0$ T, and multiple resistance jumps emerge in hysteresis as B is changed. This is the case of large U/W , which might result in multiple domains densely distributed in real space at $B = 0$ T, and the magnetic field would boost the growth of domains [Fig. 3(c)]. At the critical fields, some percolation paths suddenly disappear, which would contribute to the resistance jumps. Lastly, when D is tuned inside the correlated insulating phase [Fig. 3(d)], i.e., $R_{xx} \sim 75$ k Ω , the hysteresis effect still exists, but the resistance smoothly changes with magnetic field. The result suggests the

absence of globally preferred spin orientation for different domains at zero magnetic field. The external magnetic field provides an anisotropic energy $E = 1/2g_s\mu_B B$ by the Zeeman effect, and it tends to align the spin orientation from different domains, as shown in the bottom panel of Fig. 3(e). The presence of domains with different spin orientation might be due to the inhomogeneity of twisted angle and unexpected strain despite the most delicate sample fabrication [39–43]. A slight inhomogeneity in moiré systems alters the ground state on a microscopic scale, inducing a phase separation near the phase boundary.

E. Competing orders and abundant first-order transitions

Next, we discuss the competing orders and the resulted abundant first-order transitions in the phase diagram when the valley polarization starts to set in. Figures 4(a) and 4(b) are $R_{xx}(n, B)$ and $R_{xy}(n, B)$ color mappings at $D = -0.51$ V/nm, respectively. Here, R_{xx} and R_{xy} are symmetrically and asymmetrically processed, respectively, in order to eliminate the crosstalk (see Supplemental Material Note 1 [29]). There are four different regimes in the phase diagram, and evident phase boundaries are reflected in the Hall resistance measurements. Figure 4(c) shows three representative $R_{xy}(B)$ curves at different fillings, from which Hall carrier density (ν_H) could be obtained by linear fitting with low field data. At $\nu = 1.48$ (top panel), the linear fit by the black dashed line yields $\nu_H = 1.43$. The observation of $\nu_H \sim \nu$ indicates a fourfold degenerate Fermi surface adiabatically evolving from $\nu = 0$, a single-particle picture described by the continuum model [44,45]. At $\nu = 2.3$, the Hall carrier density follows $\nu_H \sim \nu - 2$, agreeing with a twofold degenerate Fermi surface developing from $\nu = 2$. The phase boundary between SPCIs and SPM stays unchanged in the perpendicular magnetic fields, indicating that both states

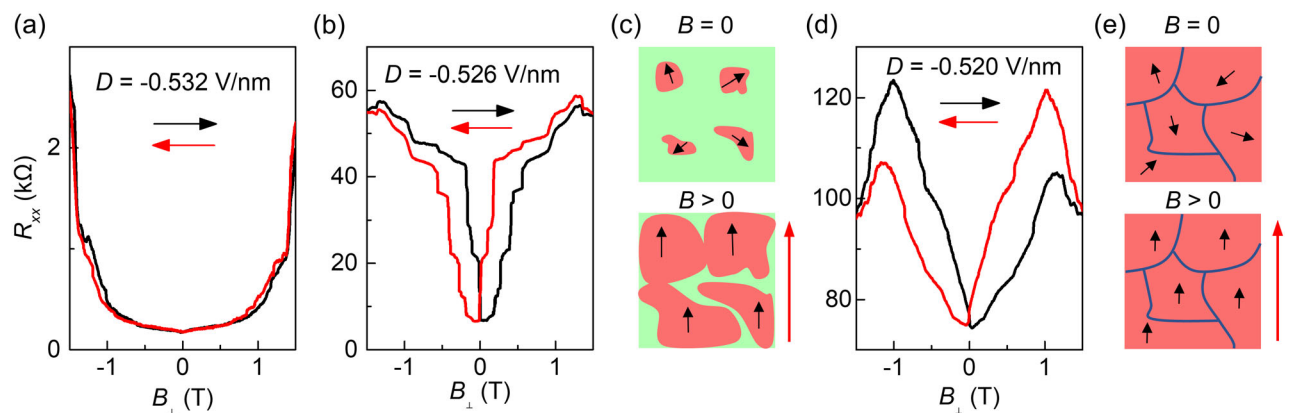


FIG. 3. Phase separation and percolation near the phase boundary. (a),(b),(d) B_{\perp} -driven hysteresis loops at different D and $T = 100$ mK. (c),(e) Schematics of phase separation and percolation. Red regions correspond to spin-polarized insulating domains, where the black arrow is the orientation of spin polarization. Green regions correspond to normal metal. The red arrow is the direction of external magnetic field.

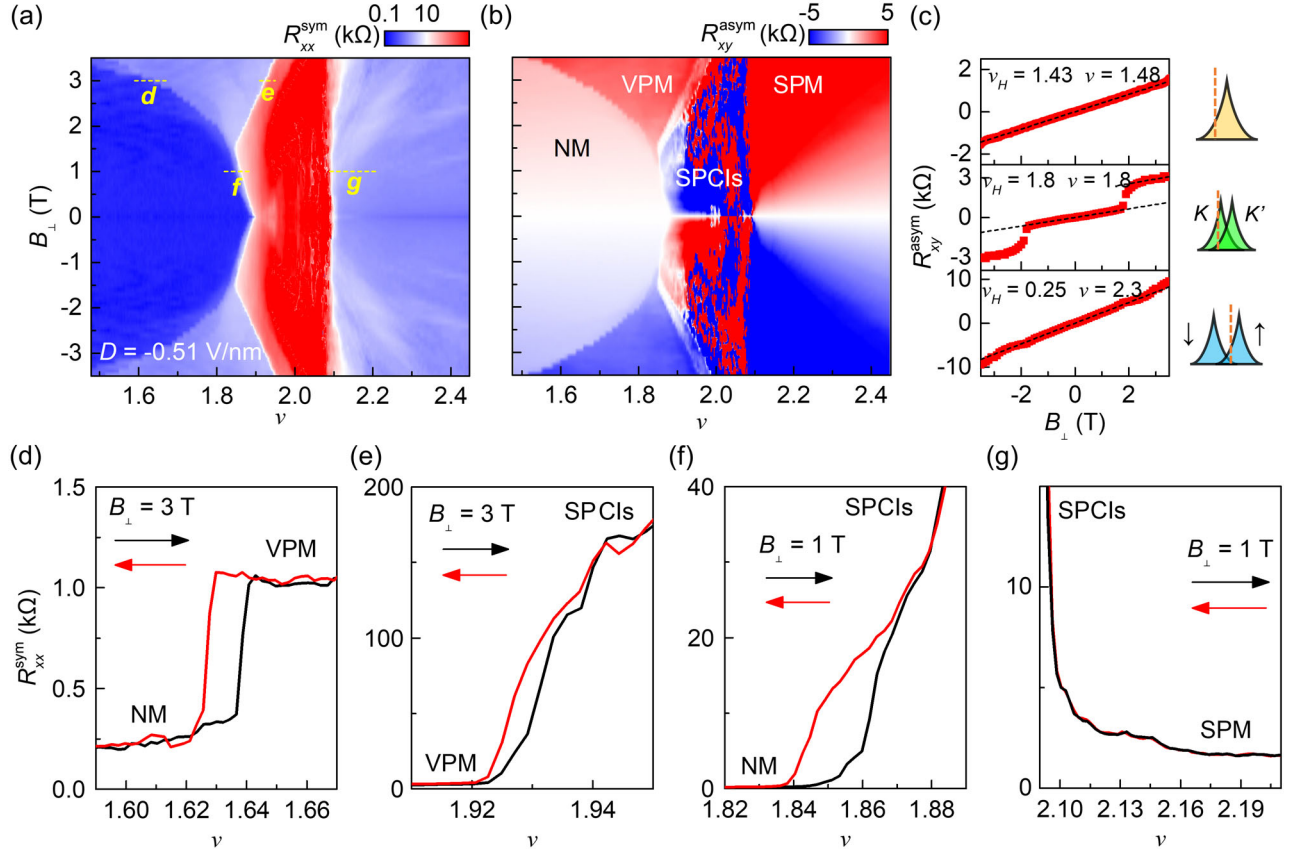


FIG. 4. Competing phase diagram and abundant first-order transitions. (a),(b) R_{xx} and R_{xy} maps as a function of ν and B_{\perp} at $D = -0.51$ V/nm. In (b), we label different phases as NM, VPM, SPCIs, and SPM. (c) R_{xy} versus B_{\perp} at different filling factors. Hall carrier densities are extracted by linear fitting. Right figures are schematics of DOS in different phases. Top panel: schematic of DOS of fourfold degenerate bands. Middle panel: schematic of DOS of valley-polarized bands. Bottom panel: schematic of DOS of spin-polarized bands. (d)–(g) Doping-driven hysteresis loops of symmetrized R_{xx} between different phases. All linecuts correspond to yellow dashed lines in (a).

are spin polarized. At $\nu = 1.8$ close to the SPCIs (middle panel), the Hall response can be divided in two parts, the ordinary Hall effect $\nu_H \sim \nu$ in low magnetic field (< 1.8 T), and the additional anomalous Hall effect in high magnetic field (> 1.8 T). The observed Hall effect follows $R_{xy} = B/(ne) + R_{xy}^A$, where the first term corresponds to the ordinary Hall effect, and the second term $R_{xy}^A \sim M$ (magnetization) represents the anomalous Hall effect [46]. Generally, the intrinsic anomalous Hall effect implies a large Berry curvature of the energy band. In TDBG, two valley-polarized sub-bands could carry opposite Chern numbers that are associated with the valley-contrasting orbital magnetism [21,44,45,47], and they are separated from each other with the increase of B_{\perp} due to the orbital Zeeman effect. Consequently, a valley-polarized (VP) state with orbital ferromagnetism and a finite Berry curvature becomes a ground state.

The competition of spin and valley is also revealed in the phase boundary between the SPCIs and VP states. At low fields $B_{\perp} < 1.35$ T, the phase boundary between SPCIs and NM extends to lower doping levels with an increasing

B_{\perp} due to the dominating spin Zeeman effect. At $B_{\perp} > 1.35$ T, VP states emerge, and it gradually takes up most of the phase space with increasing B_{\perp} . The observation suggests that VP states have lower energy than other ground states at high magnetic fields. In addition, while the phase boundary between NM and VPM keeps extending nonlinearly to a lower carrier density with increasing B , that between VPM and SPCIs shifts to a higher density almost linearly. The different tendency indicates a stronger competition of spin and valley polarization near $\nu = 2$, where the spin-polarized states resist the invasion of valley polarization. In addition, the four different phases contribute a series of phase transitions. The phase transition between NM and VPM [Fig. 4(d)] is a ferromagnetic first-order phase transition contributing abrupt resistance jumps and hysteresis. Those between VPM and SPCIs [Fig. 4(e)], as well as NM and SPCIs [Fig. 4(f)], are also a first-order transition, evident from the hysteresis. Note that all first-order transitions occur near the halo boundary, accompanied by isospin competitions. The halo boundary, also being a phase boundary with diverging DOS, gives

birth to the large isospin fluctuation that might be responsible for the first-order transition; by contrast, the transition between SPCIs and SPM is continuous and nonhysteretic [Fig. 4(g)] due to the same symmetry breaking induced by the spin polarization.

F. First-order phase transitions at quarter filling

The orbital Zeeman effect in high perpendicular magnetic field will induce fully isospin polarization near $\nu = 1$ and $\nu = 3$. As shown in Fig. 5(a), two new symmetry-breaking Fermi surfaces emanate from quarter filling at $B_{\perp} = 2$ T. Here, the value of $\nu - \nu_H$ measures the deviation of the band filling before and after the symmetry breaking, and it indicates the degree of isospin polarization [48]. The state spreading from $\nu = 2$ to $\nu = 1$ along the halo boundary corresponds to the VPM mentioned above. The linecut in Fig. 5(b) shows $\nu - \nu_H \sim 1$ (blue region), suggesting the VPM is actually the incipience of the isospin fully polarized state at $\nu = 1$. The series of Landau levels emanating from $\nu = 1$ in VPM also suggest the emerging

symmetry-breaking Fermi surface (Supplemental Material Note 10 [29]). The other state takes up the area around $\nu = 3$ and experiences a correlated gaplike transition at $\nu = 3$. The linecut also shows $\nu - \nu_H \sim 3$ [violet region in Fig. 5(b)]. These states at quarter filling are most likely the spin- and valley-polarized state (SVP) according to the theoretical calculations [35,49]. Furthermore, as shown in Figs. 5(c) and 5(d), the phase transitions between VPM and SVP (quarter filling) and SPM (half filling) with gate-voltage-driven hysteresis loops turn out to be the first-order phase transitions. The perpendicular magnetic-field-driven hysteresis loops for these two states also suggest the key role of orbital magnetization at quarter filling [11,22] [Figs. 5(e) and 5(f)].

III. CONCLUSIONS AND OUTLOOK

In TDBG, we observe correlated first-order phase transitions between SPCIs and normal metal at zero magnetic field, driven by carrier density and displacement field independently. The observations agree well with the scenario of the Lifshitz transition as well as the rapidly decreasing energy gaps at the phase boundary from Hartree-Fock calculations. These observations are important in that they unveil the long-standing mystery about the nature of the halo boundary and SPCIs [3–5,23] by providing smoking-gun evidence for the spin-polarized ferromagnetism. We also observe identical first-order metal-insulator transitions when either in-plane or out-of-plane magnetic field is applied, further demonstrating the existence of spin-polarized ferromagnetic domains. Moreover, we observe abundant competing phases and accompanied first-order phase transitions between different ground states where valley degrees of freedom play a more important role.

Our observations suggest an instability with strong isospin fluctuations near the halo boundary at high displacement field, where the combined van Hove singularity and reduced bandwidth leads to the strong Coulomb interaction effects. While the first-order transitions and the hysteresis could be captured within a picture of phase separation and percolations, more delicate theory and experiments are needed for a better understanding of this system. For instance, the first-order transitions and the hysteresis are highly tunable by electrical field and magnetic field, resembling multiferroics. The complicated flatbands in twisted multilayer systems, especially the reconstructed bands after Lifshitz transitions, might host both the electron and hole pockets, and the spatial separation of the electrons and holes at nonzero D could lead to a possible formation of electrical dipoles. In some circumstances, it might eventually form a state where spin, charge, and the layer are locked, giving birth to multiferroics in twisted multilayers. The presence of both continuous phase transition and first-order phase transition near the halo

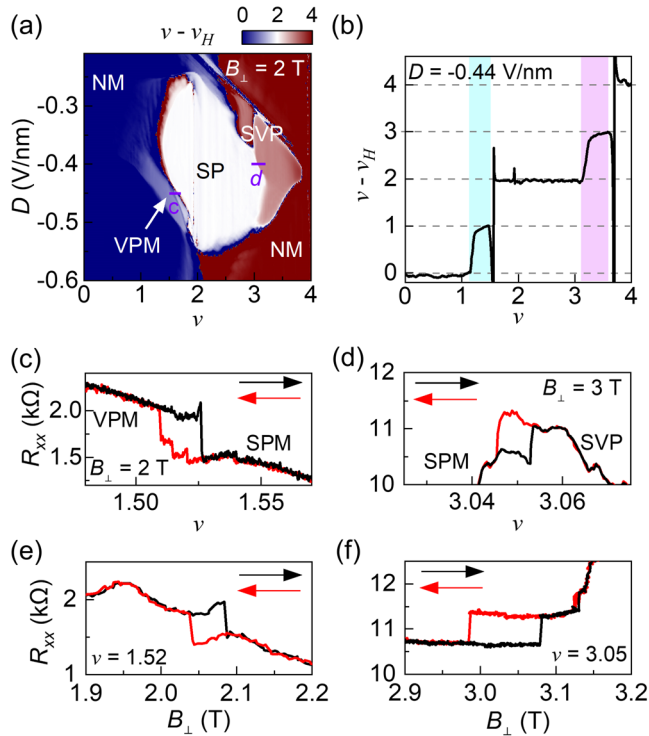


FIG. 5. First-order phase transitions and orbital magnetization at quarter fillings. (a) A color mapping of $\nu - \nu_H$ as a function of ν and D at $B_{\perp} = 2$ T. Here, SVP corresponds to spin- and valley-polarized states. (b) A linecut at $D = -0.44$ V/nm from (a). The blue region corresponds to symmetry-breaking states near $\nu = 1$, and the violet region corresponds to symmetry-breaking states near $\nu = 3$. (c),(d) Typical doping-driven hysteresis loop of R_{xx} between VPM and SPM (c) and those between SPM and SVP (d). The data in (c) and (d) correspond to the violet solid lines in (a). (e),(f) Magnetic-field-driven hysteresis loops of R_{xx} at $\nu = 1.52$ and 3.05, respectively.

boundary also deserve more investigation in TDBG as well as other twisted multilayers.

ACKNOWLEDGMENTS

We thank Kun Jiang, Zhida Song, Kam Tuen Law, Fengcheng Wu, Yu Ye, Guoqiang Yu, Erjia Guo, and Shiliang Li for useful discussions. We acknowledge support from the National Key Research and Development Program (Grants No. 2020YFA0309600 and No. 2021YFA1202900), National Natural Science Foundation of China (Grants No. 61888102, No. 11834017, and No. 12074413), the Strategic Priority Research Program of CAS (Grants No. XDB30000000 and No. XDB33000000), and the Key-Area Research and Development Program of Guangdong Province (Grant No. 2020B0101340001). J. S. acknowledges support from the Synergetic Extreme Condition User Facility at IOP, CAS. K. W. and T. T. acknowledge support from the Elemental Strategy Initiative conducted by the MEXT, Japan (Grant No. JPMXP0112101001), JSPS KAKENHI (Grants No. 19H05790, No. 20H00354, and No. 21H05233), and A3 Foresight by JSPS.

-
- [1] Y. Cao, V. Fatemi, A. Demir, S. Fang, S. L. Tomarken, J. Y. Luo, J. D. Sanchez-Yamagishi, K. Watanabe, T. Taniguchi, E. Kaxiras *et al.*, *Correlated Insulator Behaviour at Half-Filling in Magic-Angle Graphene Superlattices*, *Nature (London)* **556**, 80 (2018).
- [2] G. W. Burg, J. Zhu, T. Taniguchi, K. Watanabe, A. H. MacDonald, and E. Tutuc, *Correlated Insulating States in Twisted Double Bilayer Graphene*, *Phys. Rev. Lett.* **123**, 197702 (2019).
- [3] X. Liu, Z. Hao, E. Khalaf, J. Y. Lee, Y. Ronen, H. Yoo, D. Haei Najafabadi, K. Watanabe, T. Taniguchi, A. Vishwanath *et al.*, *Tunable Spin-Polarized Correlated States in Twisted Double Bilayer Graphene*, *Nature (London)* **583**, 221 (2020).
- [4] Y. Cao, D. Rodan-Legrain, O. Rubies-Bigorda, J. M. Park, K. Watanabe, T. Taniguchi, and P. Jarillo-Herrero, *Tunable Correlated States and Spin-Polarized Phases in Twisted Bilayer-Bilayer Graphene*, *Nature (London)* **583**, 215 (2020).
- [5] C. Shen, Y. Chu, Q. Wu, N. Li, S. Wang, Y. Zhao, J. Tang, J. Liu, J. Tian, K. Watanabe *et al.*, *Correlated States in Twisted Double Bilayer Graphene*, *Nat. Phys.* **16**, 520 (2020).
- [6] G. Chen, L. Jiang, S. Wu, B. Lyu, H. Li, B. L. Chittari, K. Watanabe, T. Taniguchi, Z. Shi, J. Jung *et al.*, *Evidence of a Gate-Tunable Mott Insulator in a Trilayer Graphene Moiré Superlattice*, *Nat. Phys.* **15**, 237 (2019).
- [7] S. Chen, M. He, Y.-H. Zhang, V. Hsieh, Z. Fei, K. Watanabe, T. Taniguchi, D. H. Cobden, X. Xu, C. R. Dean *et al.*, *Electrically Tunable Correlated and Topological States in Twisted Monolayer-Bilayer Graphene*, *Nat. Phys.* **17**, 374 (2021).
- [8] H. Polshyn, J. Zhu, M. A. Kumar, Y. Zhang, F. Yang, C. L. Tschirhart, M. Serlin, K. Watanabe, T. Taniguchi, A. H. MacDonald *et al.*, *Electrical Switching of Magnetic Order in an Orbital Chern Insulator*, *Nature (London)* **588**, 66 (2020).
- [9] S. Xu, M. M. Al Ezzi, N. Balakrishnan, A. Garcia-Ruiz, B. Tsim, C. Mullan, J. Barrier, N. Xin, B. A. Piot, T. Taniguchi *et al.*, *Tunable van Hove Singularities and Correlated States in Twisted Monolayer-Bilayer Graphene*, *Nat. Phys.* **17**, 619 (2021).
- [10] Y. Cao, V. Fatemi, S. Fang, K. Watanabe, T. Taniguchi, E. Kaxiras, and P. Jarillo-Herrero, *Unconventional Superconductivity in Magic-Angle Graphene Superlattices*, *Nature (London)* **556**, 43 (2018).
- [11] X. Lu, P. Stepanov, W. Yang, M. Xie, M. A. Aamir, I. Das, C. Urgell, K. Watanabe, T. Taniguchi, G. Zhang *et al.*, *Superconductors, Orbital Magnets and Correlated States in Magic-Angle Bilayer Graphene*, *Nature (London)* **574**, 653 (2019).
- [12] J. M. Park, Y. Cao, K. Watanabe, T. Taniguchi, and P. Jarillo-Herrero, *Tunable Strongly Coupled Superconductivity in Magic-Angle Twisted Trilayer Graphene*, *Nature (London)* **590**, 249 (2021).
- [13] G. W. Burg, E. Khalaf, Y. Wang, K. Watanabe, T. Taniguchi, and E. Tutuc, *Emergence of Correlations in Alternating Twist Quadrilayer Graphene*, *Nat. Mater.* **21**, 884 (2022).
- [14] J. M. Park, Y. Cao, L.-Q. Xia, S. Sun, K. Watanabe, T. Taniguchi, and P. Jarillo-Herrero, *Robust Superconductivity in Magic-Angle Multilayer Graphene Family*, *Nat. Mater.* **21**, 877 (2022).
- [15] Y. Zhang, R. Polski, C. Lewandowski, A. Thomson, Y. Peng, Y. Choi, H. Kim, K. Watanabe, T. Taniguchi, J. Alicea *et al.*, *Promotion of Superconductivity in Magic-Angle Graphene Multilayers*, *Science* **377**, 1538 (2022).
- [16] M. Oh, K. P. Nuckolls, D. Wong, R. L. Lee, X. Liu, K. Watanabe, T. Taniguchi, and A. Yazdani, *Evidence for Unconventional Superconductivity in Twisted Bilayer Graphene*, *Nature (London)* **600**, 240 (2021).
- [17] H. Kim, Y. Choi, C. Lewandowski, A. Thomson, Y. Zhang, R. Polski, K. Watanabe, T. Taniguchi, J. Alicea, and S. Nadj-Perge, *Evidence for Unconventional Superconductivity in Twisted Trilayer Graphene*, *Nature (London)* **606**, 494 (2022).
- [18] A. L. Sharpe, E. J. Fox, A. W. Barnard, J. Finney, K. Watanabe, T. Taniguchi, M. A. Kastner, and D. Goldhaber-Gordon, *Emergent Ferromagnetism near Three-Quarters Filling in Twisted Bilayer Graphene*, *Science* **365**, 605 (2019).
- [19] M. Serlin, C. L. Tschirhart, H. Polshyn, Y. Zhang, J. Zhu, K. Watanabe, T. Taniguchi, L. Balents, and A. F. Young, *Intrinsic Quantized Anomalous Hall Effect in a Moiré Heterostructure*, *Science* **367**, 900 (2020).
- [20] G. Chen, A. L. Sharpe, E. J. Fox, Y.-H. Zhang, S. Wang, L. Jiang, B. Lyu, H. Li, K. Watanabe, T. Taniguchi *et al.*, *Tunable Correlated Chern Insulator and Ferromagnetism in a Moiré Superlattice*, *Nature (London)* **579**, 56 (2020).
- [21] L. Liu, S. Zhang, Y. Chu, C. Shen, Y. Huang, Y. Yuan, J. Tian, J. Tang, Y. Ji, R. Yang *et al.*, *Isospin Competitions and Valley Polarized Correlated Insulators in Twisted Double Bilayer Graphene*, *Nat. Commun.* **13**, 3292 (2022).
- [22] M. Kuri, C. Coleman, Z. Gao, A. Vishnuradhan, K. Watanabe, T. Taniguchi, J. Zhu, A. H. MacDonald, and J. Folk, *Spontaneous Time-Reversal Symmetry Breaking in*

- Twisted Double Bilayer Graphene*, *Nat. Commun.* **13**, 6468 (2022).
- [23] M. He, Y. Li, J. Cai, Y. Liu, K. Watanabe, T. Taniguchi, X. Xu, and M. Yankowitz, *Symmetry Breaking in Twisted Double Bilayer Graphene*, *Nat. Phys.* **17**, 26 (2021).
- [24] D. Wong, K. P. Nuckolls, M. Oh, B. Lian, Y. Xie, S. Jeon, K. Watanabe, T. Taniguchi, B. A. Bernevig, and A. Yazdani, *Cascade of Electronic Transitions in Magic-Angle Twisted Bilayer Graphene*, *Nature (London)* **582**, 198 (2020).
- [25] U. Zondiner, A. Rozen, D. Rodan-Legrain, Y. Cao, R. Queiroz, T. Taniguchi, K. Watanabe, Y. Oreg, F. von Oppen, A. Stern *et al.*, *Cascade of Phase Transitions and Dirac Revivals in Magic-Angle Graphene*, *Nature (London)* **582**, 203 (2020).
- [26] J. M. Park, Y. Cao, K. Watanabe, T. Taniguchi, and P. Jarillo-Herrero, *Flavour Hund's Coupling, Chern Gaps and Charge Diffusivity in Moiré Graphene*, *Nature (London)* **592**, 43 (2021).
- [27] Y. Chu, L. Liu, C. Shen, J. Tian, J. Tang, Y. Zhao, J. Liu, Y. Yuan, Y. Ji, R. Yang *et al.*, *Temperature-Linear Resistivity in Twisted Double Bilayer Graphene*, *Phys. Rev. B* **106**, 035107 (2022).
- [28] M. Xie and A. H. MacDonald, *Weak-Field Hall Resistivity and Spin/Valley Flavor Symmetry Breaking in Magic-Angle Twisted Bilayer Graphene*, *Phys. Rev. Lett.* **127**, 196401 (2021).
- [29] See Supplemental Material at <http://link.aps.org/supplemental/10.1103/PhysRevX.13.031015> for theoretical calculations and additional experimental results.
- [30] H. Barkhausen, *Zwei Mit Hilfe Der Neuen Verstrker Entdeckte Erscheinungen*, *Phys. Z.* **20**, 401 (1919).
- [31] F. Wu and S. Das, *Sarma, Ferromagnetism and Superconductivity in Twisted Double Bilayer Graphene*, *Phys. Rev. B* **101**, 155149 (2020).
- [32] Y.-T. Hsu, F. Wu, and S. Das Sarma, *Topological Superconductivity, Ferromagnetism, and Valley-Polarized Phases in Moire Systems: Renormalization Group Analysis for Twisted Double Bilayer Graphene*, *Phys. Rev. B* **102**, 085103 (2020).
- [33] H. Zhou, T. Xie, A. Ghazaryan, T. Holder, J. R. Ehrets, E. M. Spanton, T. Taniguchi, K. Watanabe, E. Berg, M. Serbyn *et al.*, *Half- and Quarter-Metals in Rhombohedral Trilayer Graphene*, *Nature (London)* **598**, 429 (2021).
- [34] H. Zhou, L. Holleis, Y. Saito, L. Cohen, W. Huynh, C. L. Patterson, F. Yang, T. Taniguchi, K. Watanabe, and A. F. Young, *Isospin Magnetism and Spin-Polarized Superconductivity in Bernal Bilayer Graphene*, *Science* **375**, 774 (2022).
- [35] S. Zhang, X. Dai, and J. Liu, *Spin-Polarized Nematic Order, Quantum Valley Hall States, and Field-Tunable Topological Transitions in Twisted Multilayer Graphene Systems*, *Phys. Rev. Lett.* **128**, 026403 (2022).
- [36] M. Imada, A. Fujimori, and Y. Tokura, *Metal-Insulator Transitions*, *Rev. Mod. Phys.* **70**, 1039 (1998).
- [37] M. Fäth, S. Freisem, A. A. Menovsky, Y. Tomioka, J. Aarts, and J. A. Mydosh, *Spatially Inhomogeneous Metal-Insulator Transition in Doped Manganites*, *Science* **285**, 1540 (1999).
- [38] M. Uehara, S. Mori, C. H. Chen, and S.-W. Cheong, *Percolative Phase Separation Underlies Colossal Magnetoresistance in Mixed-Valent Manganites*, *Nature (London)* **399**, 560 (1999).
- [39] A. Uri, S. Grover, Y. Cao, J. A. Crosse, K. Bagani, D. Rodan-Legrain, Y. Myasoedov, K. Watanabe, T. Taniguchi, P. Moon *et al.*, *Mapping the Twist-Angle Disorder and Landau Levels in Magic-Angle Graphene*, *Nature (London)* **581**, 47 (2020).
- [40] T. Benschop, T. A. de Jong, P. Stepanov, X. Lu, V. Stalman, S. J. van der Molen, D. K. Efetov, and M. P. Allan, *Measuring Local Moiré Lattice Heterogeneity of Twisted Bilayer Graphene*, *Phys. Rev. Res.* **3**, 013153 (2021).
- [41] C. L. Tschirhart, M. Serlin, H. Polshyn, A. Shragai, Z. Xia, J. Zhu, Y. Zhang, K. Watanabe, T. Taniguchi, M. E. Huber *et al.*, *Imaging Orbital Ferromagnetism in a Moiré Chern Insulator*, *Science* **372**, 1323 (2021).
- [42] S. Grover, M. Bocarsly, A. Uri, P. Stepanov, G. Di Battista, I. Roy, J. Xiao, A. Y. Meltzer, Y. Myasoedov, K. Pareek *et al.*, *Chern Mosaic and Berry-Curvature Magnetism in Magic-Angle Graphene*, *Nat. Phys.* **18**, 885 (2022).
- [43] C. L. Tschirhart, E. Redekop, L. Li, T. Li, S. Jiang, T. Arp, O. Sheekey, T. Taniguchi, K. Watanabe, M. E. Huber *et al.*, *Intrinsic Spin Hall Torque in a Moiré Chern Magnet*, *Nat. Phys.* **19**, 807 (2023).
- [44] M. Koshino, *Band Structure and Topological Properties of Twisted Double Bilayer Graphene*, *Phys. Rev. B* **99**, 235406 (2019).
- [45] N. R. Chebrolu, B. L. Chittari, and J. Jung, *Flat Bands in Twisted Double Bilayer Graphene*, *Phys. Rev. B* **99**, 235417 (2019).
- [46] N. Nagaosa, J. Sinova, S. Onoda, A. H. MacDonald, and N. P. Ong, *Anomalous Hall Effect*, *Rev. Mod. Phys.* **82**, 1539 (2010).
- [47] J. Liu, Z. Ma, J. Gao, and X. Dai, *Quantum Valley Hall Effect, Orbital Magnetism, and Anomalous Hall Effect in Twisted Multilayer Graphene Systems*, *Phys. Rev. X* **9**, 031021 (2019).
- [48] Y. Saito, F. Yang, J. Ge, X. Liu, T. Taniguchi, K. Watanabe, J. I. A. Li, E. Berg, and A. F. Young, *Isospin Pomeranchuk Effect in Twisted Bilayer Graphene*, *Nature (London)* **592**, 220 (2021).
- [49] J. Y. Lee, E. Khalaf, S. Liu, X. Liu, Z. Hao, P. Kim, and A. Vishwanath, *Theory of Correlated Insulating Behaviour and Spin-Triplet Superconductivity in Twisted Double Bilayer Graphene*, *Nat. Commun.* **10**, 5333 (2019).